Mono- and Dinuclear d^{10} Metal Complexes of Hexakis(3,5-dimethylpyrazolyl)cyclotriphosphazene. Synthesis, Structures, and Unusual Solution Dynamic Behavior

Younghun Byun,[†] Dongwon Min,[†] Junghwan Do,[‡] Hoseop Yun,[‡] and Youngkyu Do*,[†]

Department of Chemistry and Center for Molecular Science, Korea Advanced Institute of Science and Technology, Taejon 305-701, Korea, and Department of Chemistry, Ajou University, Suwon 441-749, Korea

Received July 17, 1995[⊗]

Synthesis, structures, and unusual solution dynamic processes of d^{10} metal complexes of hexakis(3,5-dimethylpyrazolyl)cyclotriphosphazene (**L**) are reported. Reaction systems with three MX_n:**L** mole ratios (MX_n = d^{10} metal halide) in CH_2Cl_2 have resulted in the formation of [ICu(μ,η^3,η^3-**L**)CuI] (**1**), [Cl_2Zn(μ,η^2,η^3-**L**)ZnCl_2] (**2**), [Cl_2Cd(μ,η^3,η^3-**L**)CdCl_2] (**3**), and [(η^3-**L**)HgCl_2] (**4**). These compounds were characterized by single crystal X-ray diffraction studies, and crystallographic data are given in the order of compound: crystal system; space group; unit cell parameters; *Z*; unique data ($I > 2\sigma(I)$); R_1. **1**·0.5CH_2Cl_2: monoclinic; $P2_1/c$; a = 8.268(4) Å; b = 22.365(5) Å; c = 23.325(8) Å, β = 93.06(1)°; 4; 5736; 4.82. **2**·CH_3CN: monoclinic; $P2_1/c$; a = 17.021(3) Å; b = 12.161(2) Å; c = 23.608(5) Å; β = 107.72(1)°; 4; 5469; 3.16. **3**·CH_2Cl_2: monoclinic; $P2_1/n$; a = 18.585(5) Å; b = 17.585(4) Å; c = 14.404(3) Å; β = 102.71(2)°; 4; 3814; 3.65. The structure of **4** was attempted but resulted in data of low precision. Reaction of **L** with CuI and $ZnCl_2$ in an equimolar ratio afforded [ICu(μ,η^3,η^3-**L**)ZnCl_2] (**5**) which crystallizes in monoclinic space group $P2_1/n$ with a = 22.876(5) Å, b = 21.594(4) Å, c = 9.177(2) Å, β = 93.54(2)°, Z = 4, and R_1 = 7.00 for 3806 ($I > 2\sigma(I)$) data. In all cases, metal halide centers except the Td zinc site in **2** are coordinated by **L** via a κ^3N binding core consisting of two nongeminal pyrazolyl nitrogen atoms and one phosphazene ring nitrogen atom. The η^2-N_2 coordination in **2** involves two geminal pyrazolyl nitrogen atoms. Factors which govern the nuclearity of the complex were partially demonstrated. The intermetallic distances in dinuclear metallophosphazenes range from 6.790 to 7.195 Å. The solution behavior of five compounds was studied by variable temperature $^{31}P\{^1H\}$, ^1H, and ^{113}Cd FT NMR spectroscopy. Compounds **1** and **4** are associated with fluxional motions involving A_2B low-temperature limit spectrum while compounds **2** and **5** show solvent-dependent dynamic processes with ABX and A_2B low-temperature limit spectral patterns. Compounds **3** constitutes a fluxional system involving three A_2B species. Accounts of solution NMR spectra were attempted by using PANIC, by assuming the formation of new solution metallophosphazene species and by considering several types of dynamic processes such as a ring-around type hopping motion for the κ^3N metal site, a Td conformational change for the geminal pyrazolyl κ^2N metal site, and a wigwag motion for the nongeminal pyrazolyl κ^2N metal unit.

Introduction

Phosphazenes, inorganic hetero ring and chain compounds containing alternate phosphorus and nitrogen atoms in their skeleton, are unique carriers for transition metals owing to their ability to serve as versatile multifunctional ligands and templates.[1,2] The chemistry of metallophosphazenes, which spans the overlapped area of three materials science fields of polymers, ceramics, and metals, has been the subject of increasing research interest in conjunction with the potential opportunities for discovering new materials.[3] Among others, the use of exocyclic donor groups attached to phosphazene skeletal phosphorus appears to be the most versatile method of preparing metallophosphazenes.[4−7] For example, cyclopentadienyl-substituted cyclotriphosphazenes were successfully employed in preparing a new class of small molecule mononuclear metallophosphazenes as well as polymeric metallophosphazenes.[4]

* To whom correspondence should be addressed.
[†] Korea Advanced Institute of Science and Technology.
[‡] Ajou University.
[⊗] Abstract published in *Advance ACS Abstracts,* May 15, 1996.

(1) (a) Allcock, H. R.; Desorcie, J. L.; Riding, G. H. *Polyhedron* **1987**, *6*, 119. (b) Allcock, H. R. In *Rings, Clusters, and Polymers of the Main Group Elements*; Cowley, A. H., Ed.; ACS Symposium Series; American Chemical Society: Washington, DC, 1983; Chapter 3. (c) Allcock, H. R. *Phosphorus-Nitrogen Compounds: Cyclic, Linear and High Polymeric Systems*; Academic Press: New York and London, 1972.
(2) (a) Chandrasekhar, V.; Thomas, K. R. J. *Struct. Bonding (Berlin)* **1993**, *81*, 41. (b) Allen, C. W. *Chem. Rev.* **1991**, *91*, 133.
(3) (a) Mark, J. E.; Allcock, H. R.; West, R. *Inorganic Polymers*; Prentice-Hall Inc.: New York, 1992; Chapter 3. (b) Chandrasekhar, V.; Thomas, K. R. J. *Appl. Organomet. Chem.* **1993**, *7*, 1.
(4) (a) Allcock, H. R.; Turner, M. L. *Macromolecules* **1993**, *26*, 3. (b) Allcock, H. R.; Dodge, J. A.; Manners, I.; Parvez, M.; Riding, G. H.; Visscher, K. B. *Organometallics* **1991**, *10*, 3098. (c) Allcock, H. R.; Dodge, J. A.; Manners, I.; Riding, G. H. *J. Am. Chem. Soc.* **1991**, *113*, 9596. (d) Manners, I.; Riding, G. H.; Dodge, J. A.; Allcock, H. R. *J. Am. Chem. Soc.* **1989**, *111*, 3067. (e) Manners, I.; Coggio, W. D.; Mang, M. N.; Parvez, M.; Allcock, H. R. *J. Am. Chem. Soc.* **1989**, *111*, 3481.
(5) (a) Thomas, K. R. J.; Tharmaraj, P.; Chandrasekhar, V.; Bryan, C. D.; Cordes, A. W. *Inorg. Chem.* **1994**, *33*, 5382. (b) Thomas, K. R. J.; Tharmaraj, P.; Chandrasekhar, V.; Tiekink, E. R. T. *J. Chem. Soc., Dalton Trans.* **1994**, 1301.
(6) (a) Chandrasekaran, A.; Krishnamurthy, S. S.; Nethaji, M. *J. Chem. Soc., Dalton Trans.* **1994**, 63. (b) Chandrasekaran, A.; Krishnamurthy, S. S.; Nethaji, M. *Inorg. Chem.* **1994**, *33*, 3085. (c) Chandrasekaran, A.; Krishnamurthy, S. S.; Nethaji, M. *Inorg. Chem.* **1993**, *32*, 6102.
(7) (a) Allcock, H. R.; Nissan, R. A.; Harris, P. J.; Whittle, R. R. *Organometallics* **1984**, *3*, 432. (b) Allcock, H. R.; Lavin, K. D.; Tollefson, N. M.; Evans, T. L. *Organometallics* **1983**, *2*, 432. (c) Allcock, H. R.; Manners, I.; Mang, M. N.; Parvez, M. *Inorg. Chem.* **1990**, *29*, 522. (d) Allcock, H. R.; Scopelianos, A. G.; Whittle, R. R.; Tollefson, N. M. *J. Am. Chem. Soc.* **1983**, *105*, 1316.

S0020-1669(95)00907-4 CCC: $12.00

In particular, hexakis(3,5-dimethylpyrazolyl)cyclotriphosphazene (**L**) would be a very useful ligand system due to its multiple chelate sites but the scope of its coordination chemistry has not been well defined.[8] Recent work[9,10] on the use of the

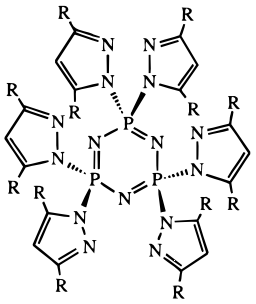

L (R = Me)

phosphazene compound **L** has been limited to the synthesis and characterization of d^9-Cu(II) complexes as well as the first fortuitous observation[10] of a structurally characterized unusual dicopper(II) complex of a pyrazolylcyclophosphazene oxide. As part of our efforts to synthesize polynuclear metallophosphazenes, prompted by the paucity of data for such a class, we have explored a wide range of reactions including d^{10}-metal ion systems. Here we elaborate on our earlier report of the homodinuclear complexation chemistry of **L** with CuI and $ZnCl_2$,[11] including its reactions with $CdCl_2$, $HgCl_2$, and a mixture of CuI/$ZnCl_2$, the structures of **L**·$(MX_n)_2$ (MX_n = CuI, $ZnCl_2$, or $CdCl_2$), **L**·$HgCl_2$, and (CuI)·**L**·($ZnCl_2$), and the unusual solution fluxionalities of these new metallophosphazenes.

Experimental Section

Preparation of Compounds. All manipulations were carried out under a pure dinitrogen atmosphere using a Vacuum Atmosphere drybox equipped with a Model HE 493 Dri-Train gas purifier or a vacuum line using standard Schlenk techniques.[12] Reagent grade solvents were distilled from appropriate drying agents[13] under a dinitrogen atmosphere, stored over activated 4A molecular sieves, and degassed prior to use. The deuterated solvents were dried before use by trap-to-trap distillation from the activated 3A molecular sieves. Triethylamine from Aldrich was treated with CaH_2 for more than 1 day, and the filtered triethylamine was distilled over CaH_2 for immediate use. Anhydrous d^{10}-metal halides, hexachlorocyclotriphosphazene, and other chemicals were purchased from Aldrich and used as received. Hexakis(3,5-dimethylpyrazolyl)cyclotriphosphazene ($P_3N_3(3,5\text{-}Me_2C_3N_2H)_6$, **L**) was prepared either by the earlier literature procedure[8] or by the recent modified method.[9]

[ICu(μ,η^3,η^3-L)CuI]·0.5CH_2Cl_2 (1·0.5CH_2Cl_2). A solid mixture of CuI (286 mg, 1.50 mmol) and **L** (352 mg, 0.5 mmol) was allowed to react in 20 mL of CH_2Cl_2. After being stirred at 25 °C for 12 h, the reaction mixture was filtered. The volume of the filtrate was reduced in vacuo, and the addition of *ca*. 30 mL of Et_2O was followed. The resulting colorless crystalline solid was collected and recrystallized from CH_2Cl_2/Et_2O, affording analytically pure product in a yield of 78% (440 mg). Anal. Calcd for $C_{30.5}H_{43}N_{15}P_3ClCu_2I_2$: C, 32.5; H, 3.84; N, 18.6. Found: C, 33.2; H, 3.90; N, 19.3. IR (KBr): 3092, 2964, 2923, 1573, 1460, 1408, 1293, 1230 (ν_{PN}), 1201 (ν_{PN}), 1155, 966, 587, 518, 453 cm^{-1}. $^{31}P\{^1H\}$-NMR (CD_2Cl_2, 297 K): δ −3.91 (s). ^1H-NMR (CD_2Cl_2, 298 K): δ 6.08 (s), 2.38 (s), 2.25 (s).

[$Cl_2Zn(\mu,\eta^2,\eta^3$-L)$ZnCl_2$]·CH_3CN (2·CH_3CN). To a slurry of $ZnCl_2$ (82 mg, 0.60 mmol) in 10 mL of CH_2Cl_2 was added a solution of **L** (141 mg, 0.20 mmol) in 20 mL of CH_2CL_2. Stirring the reaction mixture for 12 h at room temperature resulted in the precipitation of a white powder which was separated by filtration and extracted with 40 mL of acetonitrile. Treatment of the filtered acetonitrile solution with an excess amount of Et_2O gave colorless crystalline solid product. Recrystallization of this product from CH_3CN/Et_2O gave analytically pure product in a yield of 40% (82 mg). Anal. Calcd for $C_{32}H_{45}N_{16}P_3Zn_2Cl_4$: C, 37.7; H, 4.45; N, 22.0. Found: C, 37.3; H, 4.87; N, 22.0. IR (KBr): 3141, 3104, 2981, 2928, 1575, 1410, 1295, 1219 (ν_{PN}), 1199 (ν_{PN}), 1040, 953, 605, 548, 526, 472 cm^{-1}. $^{31}P\{^1H\}$-NMR (CD_3CN, 297 K): δ −0.15 (s). ^1H-NMR (CD_3CN, 297 K): δ 6.14 (s), 2.24 (s), 2.15 (s).

[$Cl_2Cd(\mu,\eta^3,\eta^3$-L)$CdCl_2$]·CH_2Cl_2 (3·CH_2Cl_2). A solution of **L** (141 mg, 0.20 mmol) in 10 mL of CH_2Cl_2 was added to a slurry of $CdCl_2$ (108 mg, 0.60 mmol) in a mixed solvent of CH_2Cl_2 (10 mL) and Et_2O (20 mL). The reaction mixture was stirred for 12 h at room temperature and filtered using a Celite pad. The filtrate was reduced in volume to *ca*. 5 mL, and 50 mL of Et_2O was added, precipitating white solids. The precipitate was collected, washed with Et_2O, and recrystallized by slow layer diffusion of Et_2O into a CH_2Cl_2 solution, affording colorless rectangular crystals (114 mg, 49% yield). Anal. Calcd for $C_{31}H_{44}N_{15}P_3Cd_2Cl_6$: C, 32.2; H, 3.83; N, 18.2. Found: C, 31.8; H, 3.62; N, 17.9. IR (KBr): 3097, 2967, 2923, 1577, 1457, 1407, 1295, 1197 (ν_{PN}), 1176 (sh, ν_{PN}), 1136, 1116, 1036, 978, 961, 896, 832, 776, 733, 601, 546, 450 cm^{-1}. $^{31}P\{^1H\}$-NMR (CD_2Cl_2, 297 K): δ 3.55 (br), −0.26 (br). ^1H-NMR (CD_2Cl_2, 297 K): δ 6.23 (br), 2.30 (br).

[$Cl_2Hg(\eta^3$-L)] (4). A mixture of $HgCl_2$ (650 mg, 2.40 mmol) and **L** (560 mg, 0.80 mmol) in 50 mL of CH_2Cl_2 was stirred for 12 h at ambient temperature. The reaction mixture was filtered, and the volume of the filtrate was reduced to *ca*. 5 mL. The addition of *n*-hexane (30 mL) to the concentrated filtrate gave a white precipitate which was collected and recrystallized from CH_2Cl_2/*n*-pentane (484 mg, 62% yield). Anal. Calcd for $C_{30}H_{42}N_{15}P_3HgCl_2$: C, 36.9; H, 4.33; N, 21.5. Found: C, 37.6; H, 4.48; N, 19.8. IR (KBr): 3102, 2969, 2924, 1572, 1297, 1214 (ν_{PN}), 1198 (ν_{PN}), 1147, 1085, 966, 600, 514 cm^{-1}. $^{31}P\{^1H\}$-NMR (CD_2Cl_2, 297 K): δ −0.68 (s). ^1H-NMR (CD_2Cl_2, 297 K): δ 6.14 (s), 2.24 (s), 2.15 (s).

[ICu(μ,η^3,η^3-L)$ZnCl_2$] (5). To a mixed slurry of CuI (38 mg, 0.2 mmol) and $ZnCl_2$ (27 mg, 0.20 mmol) in CH_2Cl_2 (20 mL) was added a solution of **L** (141 mg, 0.20 mmol) in 20 mL of CH_2Cl_2 at ambient temperature. Stirring for 12 h gave a nearly clear reaction mixture which was filtered through a Celite pad. The addition of an excess amount of Et_2O to the concentrated filtrate gave a white powdery solid. The collection of the solid was followed by double washing with Et_2O and recrystallization from CH_2Cl_2/Et_2O, affording colorless crystalline product in a yield of 76% (157 mg). A different reaction sequence of CuI with **L** and then with $ZnCl_2$ in CH_2Cl_2 with an equimolar ratio also gave the same product. Anal. Calcd for $C_{30}H_{42}N_{15}P_3CuIZnCl_2$: C, 34.9; H, 4.10; N, 20.4. Found: C, 34.1; H, 4.65; N, 19.9. IR (KBr): 3101, 2973, 2925, 1576, 1461, 1438, 1409, 1376, 1298, 1223 (ν_{PN}), 1184 (ν_{PN}), 1086, 1038, 977, 962, 897, 811, 777, 598, 536, 455 cm^{-1}. $^{31}P\{^1H\}$-NMR (CD_2Cl_2, 297 K): δ 0.21 (br), −1.51 (br), −3.94 (s). ^1H-NMR (CD_2Cl_2, 297 K): δ 6.07 (br), 2.37 (br), 2.24 (br).

X-ray Structural Determinations. Diffraction-quality crystals were obtained by diffusion of Et_2O into solutions of the compounds in CH_2Cl_2 for **1**·0.5CH_2Cl_2, **3**·CH_2Cl_2, and **5** as colorless needle, rectangular block, and rectangular block, respectively, Et_2O into a solution of **2**·CH_3CN in CH_3CN as colorless rectangular block, or *n*-pentane into a solution of **4** in CH_2Cl_2 as colorless needle. All crystals were mounted on glass fibers, and diffraction data were collected on a MAC Science MXC3 or an Enraf−Nonius CAD4 diffractometer equipped with graphite-monochromated Mo Kα radiation (0.71073 Å) operating at *ca*. 293 K. Accurate unit cell parameters and an orientation matrix were determined from the least-squares fits of accurately centered reflections (**1**·0.5CH_2Cl_2, 25 reflections with $25° \le 2\theta \le 32°$; **2**·CH_3CN, 25 with $20° \le 2\theta \le 28°$; **3**·CH_2Cl_2, 25 with $22° \le 2\theta \le 28°$; **4**, 23 with $16° \le 2\theta \le 20°$; **5**, 25 with $20° \le 2\theta \le 31°$). Intensity data were collected in the $\omega-2\theta$ scan mode for **1**·0.5CH_2Cl_2, **2**·CH_3CN,

(8) (a) Gallicano, K. D.; Paddock, N. L.; Rettig, S. J.; Trotter, J. *Inorg. Nucl. Chem. Lett.* **1979**, *15*, 417. (b) Gallicano, K. D.; Paddock, N. L. *Can. J. Chem.* **1982**, *60*, 521.
(9) Thomas, K. R. J.; Chandrasekhar, V.; Pal, P.; Scott, S. R.; Hallford, R.; Cordes, A. W. *Inorg. Chem.* **1993**, *32*, 606.
(10) Thomas, K. R. J.; Chandrasekhar, V.; Scott, S. R.; Hallford, R.; Cordes, A. W. *J. Chem. Soc., Dalton Trans.* **1993**, 2589.
(11) Min, D.; Do, Y. *Chem. Lett.* **1994**, 1989.
(12) (a) Schriver, D. F.; Drezdzon, M. A. *The Manipulation of Air-Sensitive Compounds*, 2nd ed.; John Wiley & Sons, Inc.: New York, 1986. (b) Wayda, A. L., Darensbourg, M.-Y., Eds. *Experimental Organometallic Chemistry*; ACS Symposium Series 357; American Chemical Society: Washington, DC, 1987.
(13) Perrin, D. D.; Armarego, W. L. F. *Purification of Laboratory Chemicals*, 3rd ed.; Pergamon Press: London, 1988.

Table 1. Details of Crystallographic Data[a] for **1**−**3** and **5**

	1·0.5CH_2Cl_2	**2**·CH_3CN	**3**·CH_2Cl_2	**5**
formula	$C_{30.5}H_{43}N_{15}P_3ClCu_2I_2$	$C_{32}H_{45}N_{16}P_3Cl_4Zn_2$	$C_{31}H_{44}N_{15}P_3Cl_6Cd_2$	$C_{30}H_{42}N_{15}P_3Cl_2CuZnI$
fw	1129.04	1019.29	1157.22	1032.41
crystal system	monoclinic	monoclinic	monoclinic	monoclinic
crystal dimens (mm)	0.20 × 0.15 × 0.32	0.15 × 0.10 × 0.35	0.2 × 0.3 × 0.4	0.2 × 0.2 × 0.4
space gp	$P2_1/c$ (No. 14)	$P2_1/c$ (No. 14)	$P2_1/n$ (No. 14)	$P2_1/n$ (No. 14)
a (Å)	8.268(4)	17.021(3)	18.585(5)	22.876(5)
b (Å)	22.365(5)	12.161(2)	17.585(4)	21.599(4)
c (Å)	23.325(8)	23.608(5)	14.404(3)	9.177(2)
α (deg)	90.0	90.0	90.0	90.0
β (deg)	93.06(1)	107.72(1)	102.71(2)	93.54(2)
γ (deg)	90.0	90.0	90.0	90.0
Z	4	4	4	4
cell vol (Å^3)	4307.0(27)	4654.8(15)	4592.0(19)	4495.8(16)
d_{calc} (g/cm^3)	1.741	1.454	1.674	1.525
μ (mm^{-1})	2.638	1.407	1.423	1.959
no. of obs reflns	5763 ($I \geq 2\sigma(I)$)	5469 ($I \geq 2\sigma(I)$)	3814 ($I \geq 2\sigma(I)$)	3806 ($I \geq 2\sigma(I)$)
no. of variables	499	520	526	490
R_1[b]; wR_2[c] (%)	4.82; 12.10	3.16; 8.15	3.65; 8.86	7.00; 20.06
x[c]	0.0559	0.0353	0.0528	0.1498
y[c]	20.2154	5.0534	13.7294	36.8094

[a] All data collected with graphite-monochromatized Mo Kα radiation (λ = 0.71073 Å) at 293 K. [b] $R_1 = \sum||F_o| - |F_c||/\sum|F_o|$. [c] $wR_2 = [\sum[w(F_o^2 - F_c^2)^2]/\sum[w(F_o^2)^2]]^{1/2}$, where $w = 1/[\sigma^2(F_o^2) + (xP)^2 + yP]$, $P = (F_o^2 + 2F_c^2)/3$.

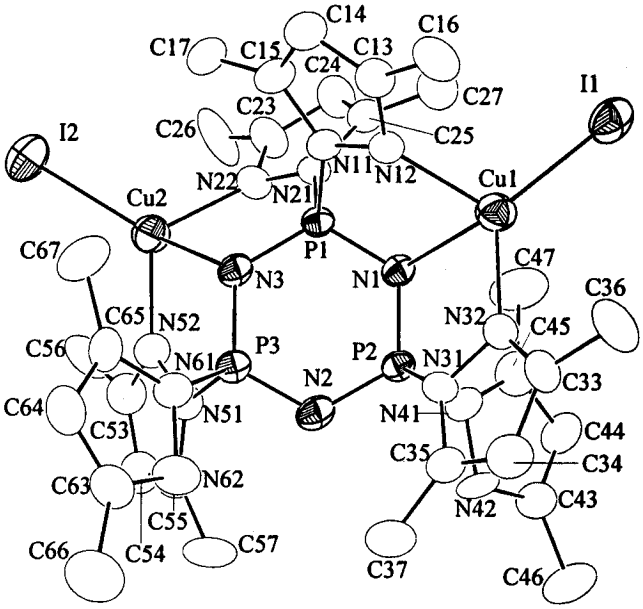

Figure 1. Molecular structure of **L**·$(CuI)_2$ (**1**) showing the atom-labeling scheme. All hydrogen atoms have been omitted for clarity.

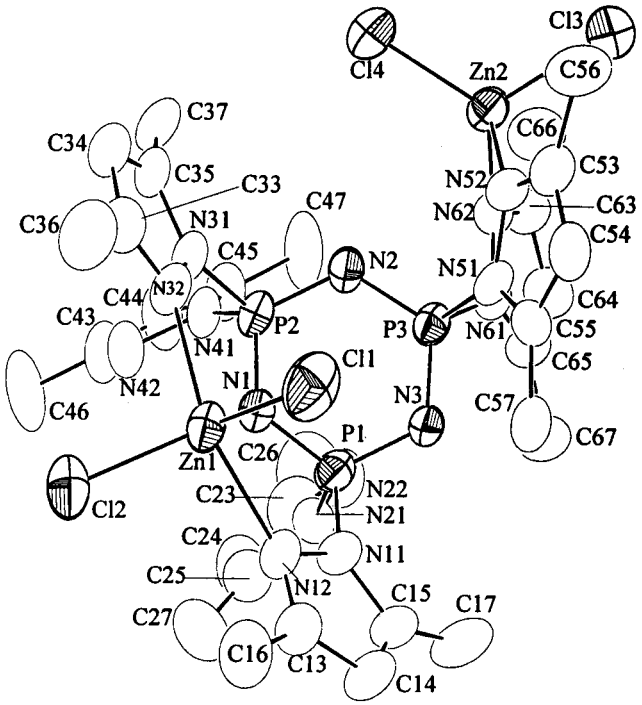

Figure 2. ORTEP diagram of **L**·$(ZnCl_2)_2$ (**2**) with hydrogen atoms omitted for clarity.

3·CH_2Cl_2, and **5** to a maximum 2θ of 48°, 45°, 40°, and 43° respectively, with the exception of **4** where the $\omega-\theta$ scan mode was used ($2\theta_{max}$ = 45°). The intensities of three standard reflections were monitored every 6000 s of exposure, and no significant decay was observed over the course of the data collection. Two standard reflections checked every 200 reflections were used to check the orientation changes of the crystal. All data sets were corrected for Lorentz and polarization effects, and empirical absorption corrections were applied using azimuthal Ψ-scan data. Systematic absences uniquely defined the space groups of all compounds.

Heavy atoms were located by use of Patterson job (SHELXS 86).[14] Atoms not located from the initial structure solution were found by successive difference Fourier maps with iterative cycles of least-squares refinement (SHELXL 93)[15] on an IBM RS/6000 workstation. All non-hydrogen atoms were treated anisotropically with the exception of those in **4**. In the case of the non-centrosymmetric system **4**, the structural refinement was attempted but resulted in data of low precision with the residual factor of R = 11.6%, and thus all structural data of **4** are deposited as Supporting Information. Full-matrix least-squares refinements were used in all cases. In the final stages of refinement, hydrogen atoms were placed at the calculated positions 0.93 or 0.96 Å from, and with isotropic thermal parameters 1.2 or 1.5 times those of, their parent carbon atoms for **1**·0.5CH_2Cl_2, **2**·CH_3CN, **3**·CH_2Cl_2, and **5**. Final difference Fourier maps showed insignificant residual electron density for **1**·0.5CH_2Cl_2, **2**·CH_3CN, and **3**·CH_2Cl_2. In the case of **5**, two residual peaks with electron density of 1.70 and 1.58 e/Å^3 separated by 2.023 Å appear at discrete positions. The presence of a fraction of methylene chloride solvent might be responsible for these peaks, but refinement of these was unsuccessful. A summary of the crystal and other data are given in Table 1, and positional and equivalent isotropic thermal parameters of the non-hydrogen atoms are deposited as Supporting Information.

Other Physical Measurements. Infrared spectra were measured as KBr pellets on a Bomem MB-100 FTIR spectrometer operating between 4000 and 350 cm^{-1} with a resolution of 4 cm^{-1} and were referenced to the 1601 cm^{-1} band of a polystyrene film. ^{1}H-NMR spectra were recorded at either 200.13 MHz on a Bruker AC 200 or

(14) Sheldrick, G. M. *SHELXS* 86. *Program for Crystal Structure Determination*; University of Göttingen: Göttingen, Germany, 1986.
(15) Sheldrick, G. M. *SHELXL 93. Program for Crystal Structural Determination*; University of Göttingen: Göttingen, Germany, 1993.

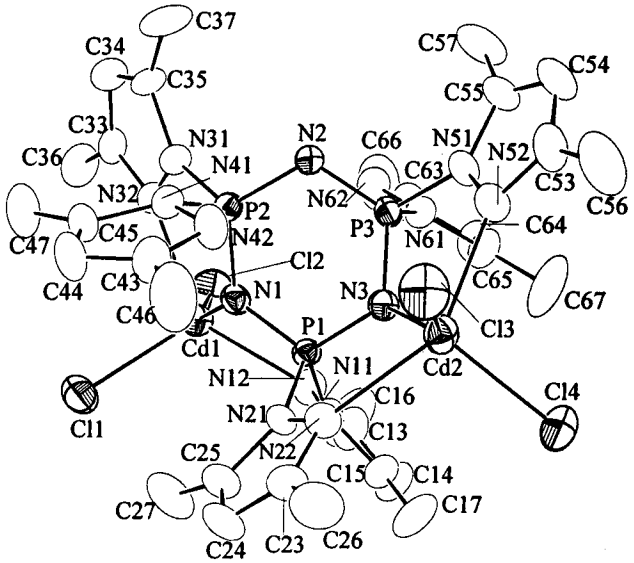

Figure 3. Molecular structure of **L**·$(CdCl_2)_2$ (**3**) showing the atom-labeling scheme. All hydrogen atoms have been omitted for clarity.

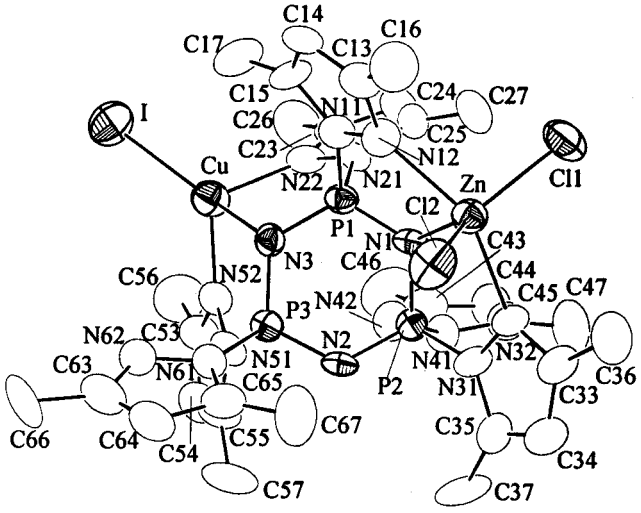

Figure 4. Molecular structure of (ICu)·**L**·$(ZnCl_2)$ (**5**) with the atom-labeling scheme.

300.13 MHz on a Bruker AM 300 spectrometer and were referenced to internal solvent peaks. $^{31}P\{^1H\}$- and ^{113}Cd-NMR spectra were obtained at 121.496 and 66.57 MHz, respectively, on a Bruker AM 300 instrument and referenced relative to external solutions of 85% H_3PO_4 and 0.1 M $Cd(ClO_4)_2$ in D_2O with positive chemical shifts referring to lower field strength. Elemental analyses for C, H, and N were performed by Han Yang Chemical Cooperation Research Center, Taejon, Korea.

Results and Discussion

Synthesis. The pyrazolyl phosphazene ligand **L** derives its ligand nature from the presence of phosphazene ring nitrogen and exocyclic pyrazolyl nitrogen atoms with competing basicity as well as from the relative steric aspects of six pyrazolyl groups. Previous failure to isolate stable di- and trinuclear copper(II) complexes of **L** has been ascribed to the lack of ligand ability to coordinate copper(II) exclusively through geminal exocyclic pyrazolyl nitrogen atoms.[10] In homonuclear systems, 3-fold amounts of metal halides were initially used in efforts to prepare trinuclear species but dinuclear complexes for CuI, $ZnCl_2$, and $CdCl_2$ and a mononuclear complex for $HgCl_2$ were isolated as pure products. The use of exact stoichiometry, 1:1 and 1:2 ligand to metal ratios for mono- and dinuclear systems, respectively, led to the decrease in yields by *ca.* 10−20%. Factors which govern the nuclearity of the complexes include the ligand nature of **L**, the nature of the transition metal involved, and the stability and solubility of complex species. The last factors were demonstrated in part in a series of separate experiments using an equimolar reaction system between CuI and **L**.

The *in situ* ^{31}P-NMR spectrum of the reaction mixture generated by stirring 1:1 CuI/**L** in $CHCl_3$ for 1 day contains

Table 2. Selected Interatomic Distances (Å) and Angles (deg) for [**L**$(CuI)_2$]·$0.5CH_2Cl_2$ (**1**·$0.5CH_2Cl_2$)

		Distances	
Cu1−N32	1.983(5)	Cu1−N12	2.065(5)
Cu1−N1	2.461(5)	Cu1−I1	2.4781(10)
Cu2−N52	2.000(5)	Cu2−N22	2.048(5)
Cu2−N3	2.472(5)	Cu2−I2	2.4792(11)
P1−N1	1.577(5)	P1−N3	1.587(5)
P1−N11	1.688(5)	P1−N21	1.697(4)
P2−N2	1.573(5)	P2−N1	1.589(5)
P2−N41	1.673(5)	P2−N31	1.694(5)
P3−N2	1.564(5)	P3−N3	1.583(5)
P3−N61	1.677(5)	P3−N51	1.699(5)
		Angles	
N32−Cu1−N12	116.1(2)	N32−Cu1−N1	81.6(2)
N12−Cu1−N1	76.0(2)	N32−Cu1−I1	128.38(15)
N12−Cu1−I1	113.17(13)	N1−Cu1−I1	125.12(11)
N52−Cu2−N22	113.6(2)	N52−Cu2−N3	79.4(2)
N22−Cu2−N3	77.3(2)	N52−Cu2−I2	122.4(2)
N22−Cu2−I2	121.78(15)	N3−Cu2−I2	125.91(11)
N1−P1−N3	118.4(2)	N1−P1−N11	105.4(2)
N3−P1−N11	112.2(2)	N1−P1−N21	112.0(2)
N3−P1−N21	106.0(2)	N11−P1−N21	101.7(2)
N2−P2−N1	117.9(2)	N2−P2−N41	111.1(3)
N1−P2−N41	106.9(2)	N2−P2−N31	107.1(3)
N1−P2−N31	108.9(2)	N41−P2−N31	104.1(2)
N2−P3−N3	118.8(2)	N2−P3−N61	110.6(3)
N3−P3−N61	107.1(2)	N2−P3−N51	106.1(3)
N3−P3−N51	107.6(2)	N61−P3−N51	106.0(2)
P1−N1−P2	121.3(3)	P1−N1−CuI	113.0(2)
P2−N1−Cu1	105.0(2)	P3−N2−P2	121.7(3)
P3−N3−P1	121.0(3)	P3−N3−Cu2	108.8(2)
P1−N3−Cu2	111.4(2)		

Table 3. Selected Interatomic Distances (Å) and Angles (deg) for [**L**$(ZnCl_2)_2$]·CH_3CN (**2**·CH_3CN)

		Distances	
Zn1−N32	2.141(6)	Zn1−N12	2.200(6)
Zn1−Cl2	2.233(3)	Zn1−Cl1	2.250(2)
Zn1−N1	2.332(6)	Zn2−N62	2.081(7)
Zn2−N52	2.092(6)	Zn2−Cl4	2.170(3)
Zn2−Cl3	2.243(3)	P1−N3	1.587(6)
P1−N1	1.596(6)	P1−N21	1.651(7)
P1−N11	1.679(7)	P2−N2	1.574(6)
P2−N1	1.595(6)	P2−N41	1.663(7)
P2−N31	1.666(6)	P3−N3	1.556(6)
P3−N2	1.580(6)	P3−N51	1.689(6)
P3−N61	1.690(7)		
		Angles	
N32−Zn1−N12	150.8(3)	N32−Zn1−Cl2	100.6(2)
N12−Zn1−Cl2	99.1(2)	N32−Zn1−Cl1	95.5(2)
N12−Zn1−Cl1	91.2(2)	Cl2−Zn1−Cl1	123.81(12)
N32−Zn1−N1	76.0(2)	N12−Zn1−N1	75.4(2)
Cl2−Zn1−N1	121.0(2)	Cl1−Zn1−N1	115.1(2)
N62−Zn2−N52	93.2(2)	N62−Zn2−Cl4	114.3(2)
N52−Zn2−Cl4	118.9(2)	N62−Zn2−Cl3	106.2(2)
N52−Zn2−Cl3	106.8(2)	Cl4−Zn2−Cl3	114.95(10)
N3−P1−N1	116.7(3)	N3−P1−N21	107.8(3)
N1−P1−N21	112.6(3)	N3−P1−N11	110.2(3)
N1−P1−N11	104.2(3)	N21−P1−N11	104.7(3)
N2−P2−N1	115.6(3)	N2−P2−N41	108.5(3)
N1−P2−N41	112.0(3)	N2−P2−N31	113.8(3)
N1−P2−N31	103.1(3)	N41−P2−N31	103.0(3)
N3−P3−N2	119.5(3)	N3−P3−N51	108.8(3)
N2−P3−N51	108.3(3)	N3−P3−N61	109.6(3)
N2−P3−N61	108.0(3)	N51−P3−N61	100.9(3)
P2−N1−P1	116.4(4)	P2−N1−Zn1	116.9(3)
P1−N1−Zn1	116.2(3)	P2−N2−P3	120.9(4)
P3−N3−P1	119.0(4)		

Table 4. Selected Interatomic Distances (Å) and Angles (deg) for [**L**$(CdCl_2)_2$]·CH_2Cl_2 (**3**·CH_2Cl_2)

	Distances		
Cd1−N32	2.347(5)	Cd1−N12	2.363(5)
Cd1−Cl2	2.435(2)	Cd1−Cl1	2.441(2)
Cd1−N1	2.601(4)	Cd2−N52	2.351(5)
Cd2−N22	2.353(5)	Cd2−Cl3	2.426(2)
Cd2−Cl4	2.438(2)	Cd2−N3	2.519(4)
P1−N1	1.593(5)	P1−N3	1.602(5)
P1−N11	1.676(5)	P1−N21	1.680(5)
P2−N2	1.575(5)	P2−N1	1.606(5)
P2−N31	1.671(5)	P2−N41	1.672(5)
P3−N2	1.576(5)	P3−N3	1.610(5)
P3−N61	1.671(5)	P3−N51	1.679(5)
	Angles		
N32−Cd1−N12	130.9(2)	N32−Cd1−Cl2	97.43(13)
N12−Cd1−Cl2	103.03(13)	N32−Cd1−Cl1	98.48(12)
N12−Cd1−Cl1	114.19(13)	Cl2−Cd1−Cl1	111.29(7)
N32−Cd1−N1	71.5(2)	N12−Cd1−N1	68.9(2)
Cl2−Cd1−N1	150.61(11)	C11−Cd1−N1	97.45(11)
N52−Cd2−N22	138.0(2)	N52−Cd2−Cl3	96.35(13)
N22−Cd2−Cl3	101.75(13)	N52−Cd2−Cl4	101.68(13)
N22−Cd2−Cl4	104.03(13)	Cl3−Cd2−Cl4	115.42(7)
N52−Cd2−N3	71.8(2)	N22−Cd2−N3	70.5(2)
Cl3−Cd2−N3	141.40(11)	Cl4−Cd2−N3	103.05(11)
N1−P1−N3	117.1(2)	N1−P1−N11	103.3(2)
N3−P1−N11	113.7(2)	N1−P1−N21	115.4(2)
N3−P1−N21	104.2(2)	N11−P1−N21	102.6(2)
N2−P2−N1	116.3(2)	N2−P2−N31	110.0(2)
N1−P2−N31	107.1(2)	N2−P2−N41	110.1(2)
N1−P2−N41	109.2(2)	N31−P2−N41	103.2(2)
N2−P3−N3	116.0(2)	N2−P3−N61	111.5(2)
N3−P3−N61	108.7(2)	N2−P3−N51	111.0(3)
N3−P3−N51	105.4(3)	N61−P3−N51	103.3(2)
P1−N1−P2	117.5(3)	P1−N1−Cd1	118.6(2)
P2−N1−Cd1	114.6(2)	P2−N2−P3	117.2(3)
P1−N3−P3	113.9(3)	P1−N3−Cd2	120.6(2)
P3−N3−Cd2	115.2(2)		

Table 5. Selected Interatomic Distances (Å) and Angles (deg) for [(ICu)**L**$(ZnCl_2)$] (**5**)

	Distances		
Zn−N32	2.131(9)	Zn−N12	2.159(10)
Zn−Cl2	2.245(3)	Zn−C11	2.260(3)
Zn−N1	2.343(9)	Cu−N52	1.982(9)
Cu−N22	2.034(10)	Cu−I	2.481(2)
P1−N3	1.556(9)	P1−N1	1.589(9)
P1−N11	1.689(9)	P1−N21	1.690(8)
P2−N2	1.551(9)	P2−N1	1.615(8)
P2−N31	1.661(10)	P2−N41	1.668(10)
P3−N2	1.566(9)	P3−N3	1.619(9)
P3−N61	1.683(9)	P3−N51	1.689(9)
	Angles		
N32−Zn−N12	147.9(4)	N32−Zn−Cl2	90.6(3)
N12−Zn−Cl2	93.4(3)	N32−Zn−Cl1	103.0(3)
N12−Zn−Cl1	101.1(3)	Cl2−Zn−Cl1	123.85(14)
N32−Zn−N1	76.1(3)	N12−Zn−N1	75.0(3)
Cl2−Zn−N1	122.5(2)	Cl1−Zn−N1	113.6(2)
N52−Cu−N22	108.2(4)	N52−Cu−I	127.9(3)
N22−Cu−I	120.4(3)	N3−P1−N1	119.5(5)
N3−P1−N11	111.5(5)	N1−P1−N11	103.8(4)
N3−P1−N21	107.2(4)	N1−P1−N21	110.3(4)
N11−P1−N21	103.3(4)	N2−P2−N1	115.6(5)
N2−P2−N31	113.0(5)	N1−P2−N31	103.8(5)
N2−P2−N41	108.7(5)	N1−P2−N41	110.7(5)
N31−P2−N41	104.6(5)	N2−P3−N3	115.9(4)
N2−P3−N61	106.8(5)	N3−P3−N61	113.1(5)
N2−P3−N51	112.0(5)	N3−P3−N51	106.7(5)
N61−P3−N51	101.4(5)	P1−N1−P2	116.2(5)
P1−N1−Zn	118.8(5)	P2−N1−Zn	113.8(4)
P2−N2−P3	123.3(5)	P1−N3−P3	120.8(5)

three signals at δ −0.93, −1.61, and −4.14 in a 1.3:8.1:1.0 ratio. The reaction mixture is quite stable as observed by the *in situ* ^{31}P-NMR spectrum of a 1 week old sample. The signals at δ −0.93 and −4.14 are due to the free ligand **L** and the dinuclear complex **L**·$(CuI)_2$ (**1**) (*vide infra*), respectively. The

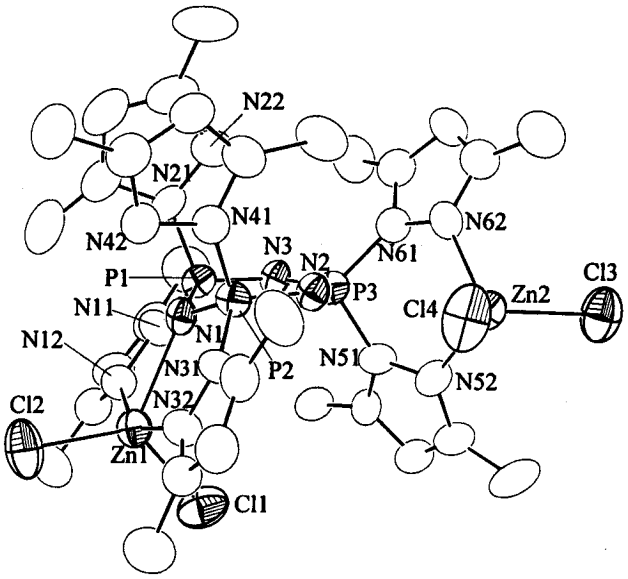

Figure 5. Perspective view of **L**·$(ZnCl_2)_2$ (**2**) revealing phosphazene ring puckering.

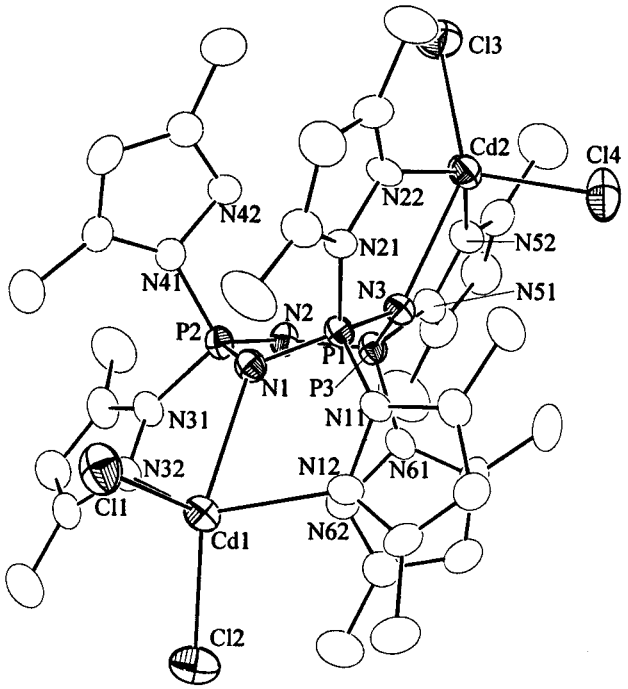

Figure 6. Perspective drawing of **L**·$(CdCl_2)_2$ (**3**) showing phosphazene ring deformation.

nature of the major signal at δ −1.61 was not clearly determined, but the mononuclear species **L**·CuI is presumably responsible for the signal. The successive addition of Et_2O into the reaction mixture afforded the isolation of pure colorless crystalline **1** as the least soluble first crop, pure free ligand **L** as the second crop, and a crystalline mixture of **L** and mononuclear **L**·CuI as the most soluble crop.[16] The isolation of pure mononuclear species by fractional recrystallization was hampered by the co-precipitation of **L**.

In the case of the heteronuclear system, the use of an equimolar stoichiometric reaction of reagents, summarized in eq 1, was successfully employed in preparing the hetero

(16) The ^{1}H- and ^{31}P-NMR spectra of the authentic samples of **L** and **L**·$(CuI)_2$ were used to characterize the crystalline precipitates. The isolation of pure **L**·(CuI) by fractional recrystallization was not successful, but its NMR spectra (in $CDCl_3$) are assigned as follows: ^{31}P-NMR, δ −1.61; ^{1}H-NMR, δ 5.89, 2.24, and 2.21. *cf.* NMR data ($CDCl_3$) of **L**: ^{31}P-NMR, δ −0.93; ^{1}H-NMR, δ 5.79, 2.16, and 2.09.

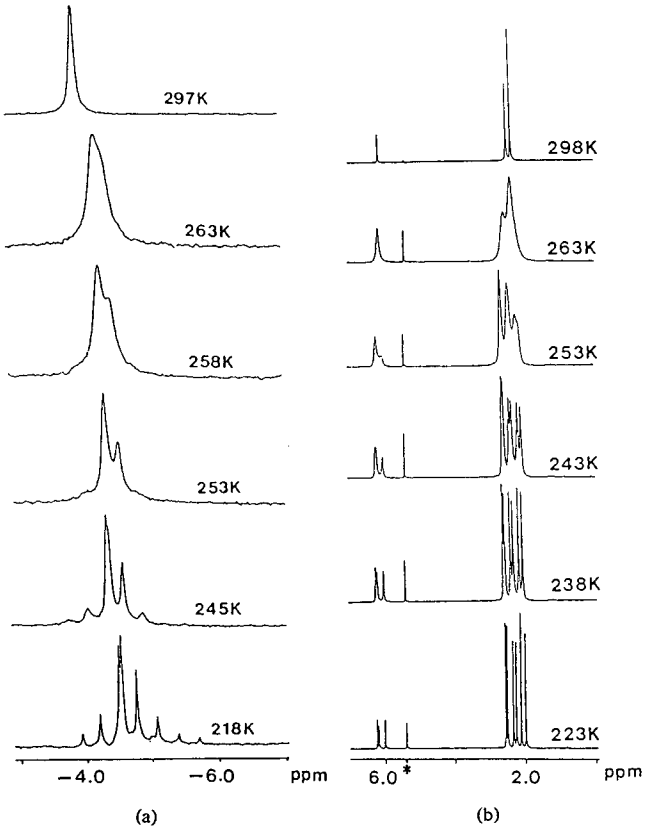

Figure 7. Varible temperature (a) $^{31}P\{^1H\}$ and (b) ^1H FT NMR spectra of **1** in CD_2Cl_2. The signal marked with an asterisk is due to the residual solvent protons.

Table 6. Summary of ^{31}P-NMR PANIC Parameters for **1**−**5**

	NMR solvent	temp. (K)	δ_A (ppm)	δ_B (ppm)	δ_X (ppm)	J_{AB} (Hz)	J_{AX} (Hz)	J_{BX} (Hz)
1·0.5CH_2Cl_2	CD_2Cl_2	188	−4.37	−5.06		60		
2·CH_3CN	CD_2Cl_2	243	1.91	−0.95		47		
			1.91	−3.31		54		
2·CH_3CN	CD_2Cl_2	203	−1.54	−1.77		48		
			−6.34	−3.59	5.89	66	42	53
2·CH_3CN	acetone-d_6	188	−1.03	−1.90		50		
3·CH_2Cl_2	CD_2Cl_2	188	−7.80	−0.75		55		
4	CD_2Cl_2	188	−2.41	−3.57		61		
5	CD_2Cl_2	233	−4.27	−4.94		68		
			−3.49	−1.87	3.15	63	44	47
5	CD_3CN	297	−0.49[a]	−1.89[a]				

[a] Broad signals.

dinuclear compound **5**. The addition of **L** to a slurry of CuI

$$\mathbf{L} + MX_n + M'X'_m \xrightarrow{CH_2Cl_2} [X_nM(\mu\text{-}\mathbf{L})M'X'_m] \qquad (1)$$

and $ZnCl_2$ in CH_2Cl_2 or the addition of $ZnCl_2$ to a clear reaction solution generated by stirring a slurry of CuI in CH_2Cl_2 for 8 h gave the same pure compound. Equation 1 was further utilized to synthesize a set of hetero dinuclear complexes [ICu(μ-**L**)$MnCl_2$], [ICu(μ-**L**)$CoCl_2$], [Cl_2Zn(μ-**L**)$CoCl_2$], and [$(CO)_3Mo$-(μ-**L**)$CoCl_2$].[17]

Structural Analysis. The phosphazene ring P−N stretching frequencies for all five complexes appear as two splitted peaks, one between 1230 and 1197 cm^{-1}, and the other between 1201 and 1176 cm^{-1}, indicating that the phosphazene ring nitrogen atoms are involved in coordination to the metal centers. Double appearance of the ν_{PN} peaks can be informatively compared with the single ν_{PN} peak of **L** at 1226 cm^{-1} regarding the effect of metalation on the phosphazene ring structure. The results of structural analysis by single crystal X-ray diffraction studies are consistent with the vibrational observation. The molecular structures and selected interatomic distances and angles for four compounds are given in Figures 1−4 and Tables 2−5, respectively. In the case of **4**, owing to the low-precision data, discussion of metric values will not be made further. Nevertheless, the results, deposited as Supporting Information, clearly establish the mononuclear nature of **4** of which the structure is analogous to that of [$Cl_2Cu(\eta^3$-**L**)].[9]

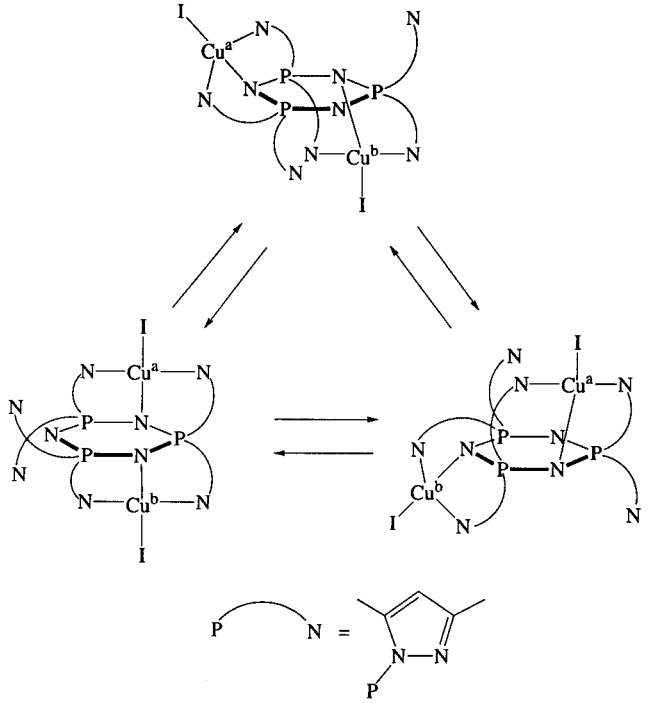

Figure 8. Solution fluxional motions of **1** in CD_2Cl_2 showing simultaneous ring-around type hopping of two copper centers. Possible stepwise hoppings involving one copper center are omitted for clarity.

(a) [ICu(μ,η^3,η^3-L)CuI]·0.5CH_2Cl_2 (1·0.5CH_2Cl_2). The molecular structure of **1** approaches C_2 symmetry and reveals that the pyrazolyl phosphazene ligand **L** bridges two copper atoms with a separation of 6.790(2) Å via two κ^3N ligating sites. Each N_3 binding core consists of one phosphazene ring nitrogen (N_{ring}) atom and two nongeminal pyrazolyl nitrogen (N_{pyz}) atoms, imposing a distortion on the metal coordination sphere. The average $N_{pyz}-Cu-N_{pyz}$ and $N_{pyz}-Cu-N_{ring}$ values are 114.9(13)° and 78.6(11)°, respectively. Both copper atoms in distorted tetrahedral local sites situate on two opposite sides of a P_3N_3 phosphazene ring which remains undistorted in spite of the coordination of two phosphazene ring nitrogen atoms to copper atoms. Small displacements of N1 (+0.056 Å) and N3 (−0.049 Å) from a mean plane defined by P1, P2, P3, and N2 reflect the planarity of the phosphazene ring.

Copper atoms interact more strongly with the ligand **L** via the pyridinic nitrogen atoms than via the phosphazene ring nitrogen atoms; the average $Cu-N_{pyz}$ distance of 2.024(17) Å is smaller than the average $Cu-N_{ring}$ distance of 2.467(5) Å. The $P-N_{ring}$ bond distances (average 1.584 Å) involving nitrogen atoms coordinated to copper atoms are slightly longer than other $P-N_{ring}$ bond lengths (average 1.569 Å), indicating that the interactions between copper atoms and phosphazene ring nitrogen atoms are weaker. This feature is consistent with previous observations[9,18] and interpretation.[19] Exocyclic $P-N_{pyz}$

(17) All compounds were well characterized, and a manuscript is in preparation for submission to *Inorg. Chem.*

(18) Krishnamurthy, S. S.; Sau, A. C.; Woods, M. *Adv. Inorg. Chem. Radiochem.* **1978**, *21*, 41.

(19) (a) Craig, D. P.; Paddock, N. L. *Nature* **1958**, *181*, 1052. (b) Craig, D. P.; Mitchell, K. A. R. *J. Chem. Soc.* **1965**, 4682.

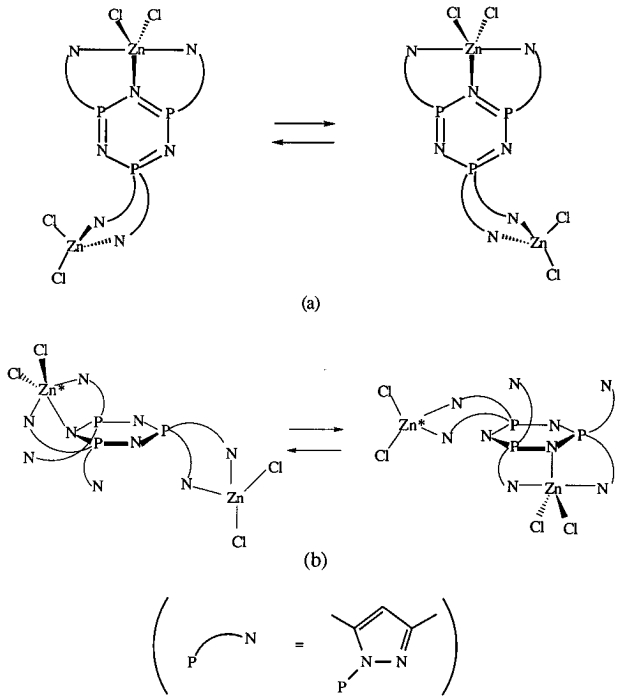

Figure 9. Schematic representation of (a) the conformational change of the Td zinc site and (b) the simultaneous conversion of TBP/Td sites of **2** in acetone.

bond lengths (average 1.695 Å) involving the coordinating pyrazolyl groups are also slightly longer than those (average 1.675 Å) involving the noncoordinating pyrazolyl groups.

(b) [$Cl_2Zn(\mu,\eta^2,\eta^3$-L)$ZnCl_2$]·CH_3CN (2·CH_3CN). The structure of **2** shows no overall symmetry and has several unprecedented features. The compound **2** constitutes the first example of dinuclear zinc phosphazene in which the ligand **L** bridges two $ZnCl_2$ units separated by 7.051 Å via a geminal pyrazolyl η^2-N_2 core and an η^3-N_3 bite similar to that in **1**, giving distorted tetrahedral (Td) and trigonal bipyramidal (TBP) geometry around zinc atoms, respectively. Metric analysis suggests that the distortions in the coordination spheres of **1** and **2** are presumably due to the steric constraints imposed by the ligand nature of **L**, and the degree of distortion is particularly large where the η^3-N_3 chelate core is involved. These are partly reflected in relatively invariable $N_{pyz}-M-N_{ring}$ angles of 78.6° (M = Cu) and 76.5° (M = Zn) for **1** and **2**, respectively.

The effect of complexation on the P_3N_3 phosphazene ring structure in **2** is rather unique. In contrast to the planar P_3N_3 nature in **1**, ring puckering toward the TBP zinc site is evident in **2**, as illustrated in Figure 5; the displacement of the N1 atom (−0.490 Å) from the plane defined by P1, P2, P3, N2, and N3 and the dihedral angle of 35.9° between the P1−N1−P2 plane and the P1−N3−P3−N2−P2 plane reflect the extent of ring deformation. The coordination effect on the $P-N_{ring}$ bonds appears as a slight lengthening of the $P-N_{ring}$ bond length (average 1.594 vs 1.579 Å) where the N_{ring} atom is involved in the coordination. This observation suggests[9,18] the presence of a weaker interaction between zinc and the N_{ring} atom, but the $Zn-N_{ring}$ interaction seems to be stronger than the $Cu-N_{ring}$ interaction in **1** as judged by considering the $M-N_{ring}$ distances of 2.298 Å (M = Zn) and 2.467 Å (M = Cu) and the ionic radii of four-coordinated Cu^+ (0.74 Å) and five-coordinated Zn^{2+} (0.82 Å).[20]

(c) [$Cl_2Cd(\mu,\eta^3,\eta^3$-L)$CdCl_2$]·CH_2Cl_2 (3·CH_2Cl_2). The ligand nature of **L** in **3** and the overall molecular symmetry are analogous to those seen in **1** but are quite different from the lighter congener compound **2**. On the other hand, the P_3N_3 ring deformation caused by metalation is similar to that in **2** as depicted in Figure 6. Two ring nitrogen atoms N1 and N3 are displaced toward two distorted TBP cadmium sites from the best plane of P1−P2−P3−N2 by +0.517 and −0.492 Å, respectively. The intercadmium Cd···Cd distance is 7.195 Å.

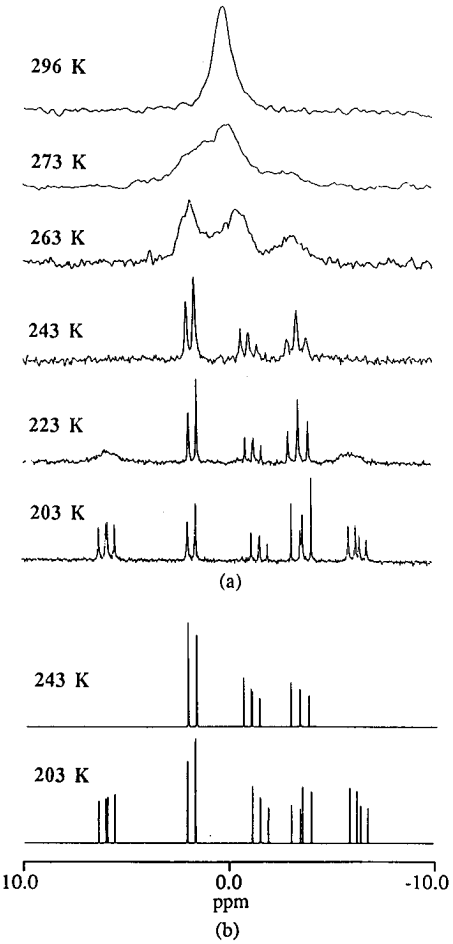

Figure 10. (a) Variable temperature $^{31}P\{^1H\}$ FT NMR spectra of **2** in CD_2Cl_2 and (b) selected PANIC spectra.

(d) [$ICu(\mu,\eta^3,\eta^3$-L)$ZnCl_2$] (5). The X-ray analysis clearly reveals an unprecedented hetero dinuclear nature of **5** which constitutes the first example of such class. It is interesting to note that the ligand **L** employs two κ^3N binding cores to coordinate metal units instead of one κ^3N core for CuI and one κ^2N core for $ZnCl_2$. The CuI and $ZnCl_2$ units are separated by 6.798 Å. Upon binding each metal exerts a different effect on the phosphazene ring deformation. For CuI binding, no ring deformation such as seen in **1** is observed and for $ZnCl_2$ binding; similar ring puckering to that found in **2** is also present in **5**.

The interaction of each metal unit with the phosphazene ring nitrogen atom in **5** is weaker than that in the homo dinuclear complex **1** or **2**. The lengthening of the $M-N_{ring}$ distances in **5** is presumably due to the presence of another metal center competitively seeking the lone pair electron density of the phosphazene ring nitrogen atoms. Particularly the lengthening of $Cu-N_{ring}$ in **5** compared to **1** suggests that the $ZnCl_2$ unit is a stronger Lewis acid than the CuI unit.

Solution Fluxionality. One of the most unusual properties of the five d^{10}-metallophosphazenes described in this paper is their complex dynamic behavior in solution. The solution fluxionality greatly depends on the type of complex as well as on the solvent and will be described in the order of increasing complexity.

(a) Systems Involving an A_2B Low-Temperature Limit Spectrum. The X-ray structures suggest that the compounds

(20) Shannon, R. D. *Acta Crystallogr.* **1976**, *A32*, 751.

1 and **4** can have C_2 and C_s solution symmetry, respectively, via the rotation of the uncoordinated pyrazolyl groups. In fact, both species in CD_2Cl_2 show A_2B $^{31}P\{^1H\}$-NMR spectra[21] at the low-temperature limit. The chemical shifts and coupling constant were determined by using PANIC (parameter adjustment in NMR by iterative calculation),[21] and the PANIC parameters for all five compounds are summarized in Table 6.

Upon increasing the temperature, both A_2B patterns begin to disappear to give a single phosphazene signal at the high-temperature limit (see Figure 7a and ref 21). Since the position of the single signal for both compounds is different from that of the free ligand **L** and due to the appearance of a single signal for **L** at 193 K, dissociation of metal halide unit(s) can be ruled out. The evidence at hand does not unequivocally reveal the solution behavior of **1** and **4** which can account for the appearance of single phosphorus signal, but the dynamic nature involving ring-around type hopping motions of metal halide unit(s) via η^3-N_3 coordination can be suggested as illustrated in Figure 8 for **1**. The change in the number of pyrazolyl 4-H proton signals around 6.1 ppm and methyl group signals around 2.5 ppm observed in variable temperature ^1H FT NMR spectra (Figure 7b) is also consistent with the solution behavior described above.

(b) Systems Showing Solvent-Dependent Fluxionalities with ABX and A_2B Low-Temperature Limit Spectral Patterns. Compounds **2** and **5** constitute unusual fluxional systems involving at least two species in solution as well as solvent dependency. Variable temperature $^{31}P\{^1H\}$ FT NMR spectra[21] of **2** in acetone are similar to the systems **1** and **4** in CD_2Cl_2 and indicative of the involvement of one species in fluxional motions. It is interesting to note that the low-temperature limit spectrum is an A_2B pattern (see Table 6) instead of an ABX pattern predicted by the solid state structure depicted in Figure 2, indicating that a fluxional motion is still operative as low as 188 K. Since it is likely that TBP−Td zinc sites observed in the solid state structure are present in the solution state, the A_2B nature can be best accounted by a fast conformational change of the Td site as illustrated in Figure 9a. The molecular model of **2** demonstrates the easiness of such change. Upon increasing the temperature, another dynamic motion which makes all phosphorus atoms magnetically equivalent begins to appear. Fast simultaneous conversion of a TBP zinc site into a Td zinc site and a Td zinc site into a TBP zinc site, schematically summarized in Figure 9b, can be reasonably suggested as a possible dynamic process of **2** in acetone.

In dichloromethane, compound **2** shows rather complex solution behavior involving two types of zinc phosphazenes as observed by variable temperature $^{31}P\{^1H\}$ FT NMR and PANIC spectra (see Figure 10). The spectrum at the low-temperature limit 203 K consists of signals due to an A_2B and an ABX species while the 243 K spectrum suggests the presence of two A_2B patterns. The number of ^1H signals[21] due to pyrazolyl 4-H protons and 3,5-dimethyl protons is consistent with the presence of A_2B and ABX species at 193 K. These observations can be described by considering the presence of another dizinc phosphazene species **2a** in addition to **2**. The TBP zinc site of **2a**

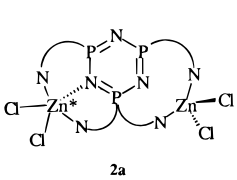

2a

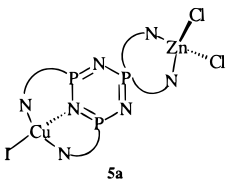

5a

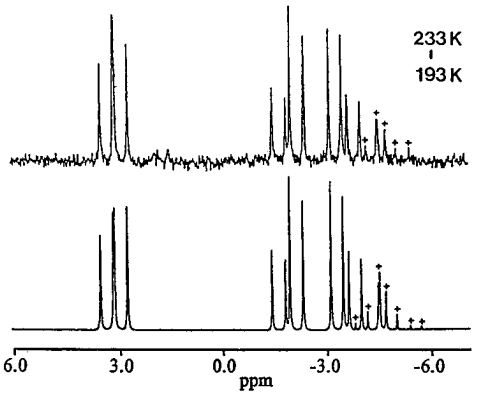

Figure 11. Comparison of the observed low-temperature limit spectrum (upper) with PANIC spectrum (lower) of **5** in CD_2Cl_2.

is the same as that of **2**, but the Td zinc site of **2a** is different from that in **2** and involves two nongeminal pyrazolyl nitrogen atoms instead of two geminal pyrazolyl nitrogen atoms. **2a** is likely to give an ABX spectrum at the low-temperature limit, and the Td zinc unit is likely to undergo a wigwag type motion[21] upon increasing the temperature, yielding an A_2B spectrum. At the higher temperature limit the TBP zinc unit also becomes fluxional[21] to make ring phosphazene atoms of **2a** magnetically equivalent.

Variable temperature $^{31}P\{^1H\}$ FT NMR spectra[21] of **5** in CD_2Cl_2 reveal the low-temperature limit spectrum, displayed in Figure 11 along with the PANIC spectrum, consisting of two sets of signals; one A_2B set with plus marks and the other ABX set without a mark in a 1:4 ratio. The solution structure of the species responsible for the ABX pattern at 193 K is believed to be the same as the solid structure with C_1 symmetry. Increasing the temperature causes both CuI and $ZnCl_2$ units to be fluxional as similarly observed for the system **1**. A complete change of ABX signals into a single peak was not observed even at 328 K. To account for the A_2B set with plus marks, the presence of a new solution complex **5a**, among other conceivable candidates, and its fluxionality similar to that of compound **2** can be reasonably suggested. The ^1H FT NMR spectra[21] of **5** in CD_2Cl_2 are also in accord with the foregoing description.

In contrast to the behavior in CD_2Cl_2, compound **5** appears as one species in CD_3CN as indicated by the $^{31}P\{^1H\}$-NMR spectra. At room temperature, the spectrum in CD_3CN is similar to the portion of the ABX pattern in CD_2Cl_2 although no indication for the appearance of the complete ABX pattern is seen as low as near the freezing point of the solvent. The solution structure of **5** in CD_3CN appears to be the same as the solid state structure.

(c) A Fluxional System Involving at Least Three A_2B Species. The dinuclear cadmium complex **3** in dichloromethane reveals very unusual solution behavior. A subtle existence of A_2B and A'_2B' $^{31}P\{^1H\}$-NMR spectra in the high-temperature range becomes evident at 253 K along with the appearance of the third A''_2B'' pattern as shown in Figure 12a. The involvement of three solution species is competing at 233 K and lasts to as low as 188 K, but the dominance of the A''_2B'' pattern at the expense of the other two patterns is seen upon decreasing temperature. Shown in Figure 13 are three possible dicadmium solution species whose fluxional motions are similar to those of previously discussed analogous metallophosphazenes and that lead to A_2B spectra. Contrary to the number of species involved in $^{31}P\{^1H\}$-NMR spectra, the ^{113}Cd-NMR spectra of **3** given in Figure 12b show only one signal at 298 and 193 K and two peaks at 233 K. Although the origin for this apparent

(21) Related figures and illustrations are deposited as Supporting Information.

(22) (a) Summers, M. F.; Marzill, L. G. *Inorg. Chem.* **1984**, *23*, 523. (b) Munakata, M.; Kitagawa, S.; Yagi, F. *Inorg. Chem.* **1986**, *25*, 964.

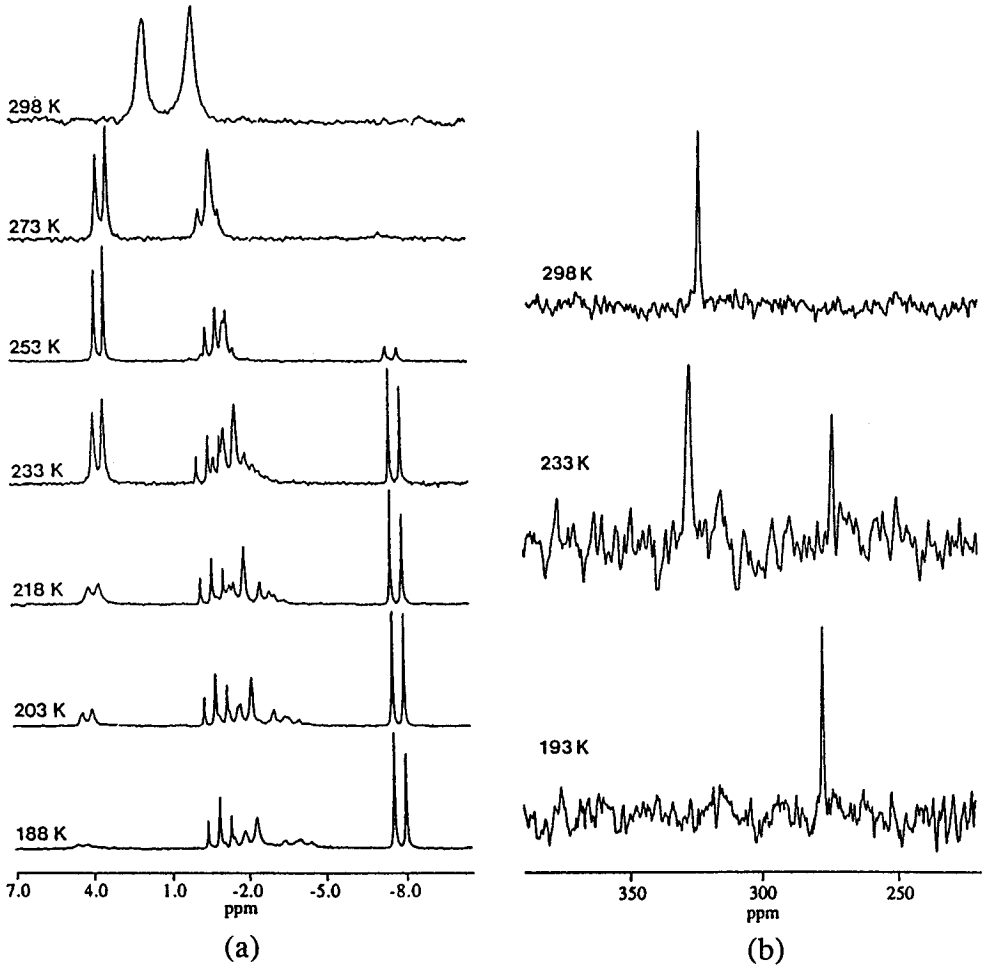

Figure 12. Variable temperature (a) $^{31}P\{^{1}H\}$ and (b) ^{113}Cd FT NMR spectra of **3** in CD_2Cl_2.

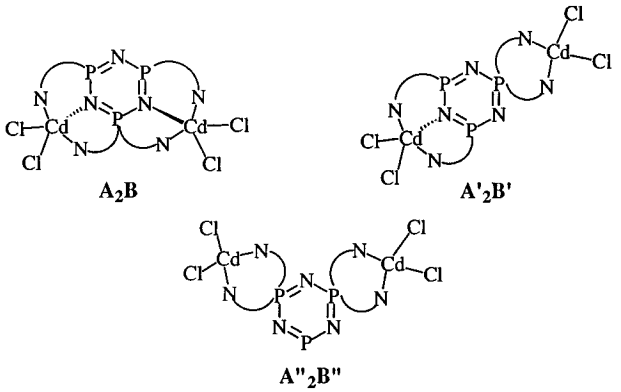

Figure 13. Three possible dicadmium solution species whose fluxional motions lead to A_2B spectra.

inconsistency between $^{31}P\{^{1}H\}$ and ^{113}Cd FT NMR spectra remains speculative, the appearance of a new signal at *ca*. 50 ppm upfield of the initial signal at 328 ppm strongly indicates[22] that the number of nitrogen donor atoms in A''_2B'' cadmium centers is less by one compared to that in A_2B cadmium centers as reflected in Figure 13.

Conclusions

Although the number of metal complexes of hexakis(3,5-dimethylpyrazolyl)cyclotriphosphazene (**L**) observed to date is quite limited, the coordination nature of **L** seems to be overwhelmed by κ^3N binding behavior involving two nongeminal pyrazolyl nitrogen atoms and a phosphazene ring nitrogen atom. Surprisingly, the binding mode of κ^2N involving two more basic geminal pyrazolyl nitrogen atoms is not common in the solid state. The reported five compounds constitute unique examples of metallophosphazenes in a sense that all show different types of unusual solution properties including the generation of new dinuclear metallophosphazenes in the solution state.

Acknowledgment. We gratefully acknowledge financial support provided by NON-DIRECTED RESEARCH FUND, Korea Research Foundation, 1993 and 1994 and by the Korea Science and Engineering Foundation.

Supporting Information Available: Tables of anisotropic thermal parameters, positional and equivalent isotropic thermal parameters, complete bond distances and angles, and calculated hydrogen atom positions for the compounds in Table 1 and figures showing additional NMR spectra, an ORTEP diagram of **4**, a wigwag type movement of a Td site, and simultaneous ring-around hopping of two zinc centers (44 pages). Ordering information is given on any current masthead page.

IC950907B